The vibrational spectrum of deuterated phosphaethyne: A quantum mechanical, classical, and semiclassical analysis

J. Bredenbeck, C. Beck, and R. Schinke[a)]
Max-Planck-Institut für Strömungsforschung, D-37073 Göttingen, Germany

J. Koput
Department of Chemistry, Adam Mickiewicz University, 60-780 Poznań, Poland

S. Stamatiadis and S. C. Farantos
Institute of Electronic Structure and Laser Foundation for Research and Technology–Hellas, Greece, and Department of Chemistry, University of Crete, Iraklion 711 10, Crete, Greece

M. Joyeux
Laboratoire de Spectrométrie Physique, Université Joseph Fourier–Grenoble I, BP 87, F-38402 St. Martin d'Heres Cedex, France

(Received 22 November 1999; accepted 28 February 2000)

The vibrational spectrum of deuterated phosphaethyne (DCP) is analyzed in terms of quantum-mechanical variational calculations, classical mechanics (periodic orbits), and an effective Hamiltonian model. The quantum mechanical and classical calculations are performed with a new, spectroscopically accurate potential energy surface. The spectrum is governed by a 2:1 DC stretch:CP stretch anharmonic resonance, which already exists for the fundamentals. The bending degree of freedom is to a large extent decoupled. It is shown that several bifurcations in the classical phase space profoundly influence the quantum spectrum. For example, a new progression, which does not exist at very low excitation energies, comes into existence at intermediate energies. In contrast to HCP, the pure bending states gradually evolve along the isomerization path with increasing bending quantum number. © *2000 American Institute of Physics.* [S0021-9606(00)00120-3]

I. INTRODUCTION

As a consequence of the coupling between the various internal modes, which typically increases with energy, the vibrational spectrum of even a triatomic molecule can become quite intricate.[1–3] In many cases, anharmonic resonances and the resulting mixing between zero-order states determine the structure of the energy spectrum even at low energies.[4–7] As a consequence of anharmonic resonances nonlinear dynamics effects such as bifurcations may occur,[8] which leave distinct hallmarks in the quantum-mechanical energy spectrum. The investigation of these and related effects reveals a lot of information about the intramolecular dynamics of small molecules, in particular, and nonlinear dynamics in general.

In a series of recent papers we analyzed, inspired by high-resolution stimulated-emission-pumping (SEP) spectroscopic measurements at high-transition energies,[9] the vibrational spectrum of HCP,[10,11] a molecule with a pronounced 2:1 CP stretch:bend resonance. The most interesting feature in the spectrum of HCP is the occurrence of a saddle-node bifurcation at relatively high energies, at which a new kind of states, which does not exist at low energies, is abruptly born. The existence of these ''isomerization'' states, as they are called,[12] has been confirmed in subsequent experiments by Ishikawa *et al.*[13] However, the early calculations were performed with a potential energy surface (PES),[10,11] which did not allow direct comparison with the experimental data. A completely new PES has been calculated by *ab initio* methods, which has the required accuracy.[14] The calculated energy levels agree very nicely with the measured ones, up to high energies, and in particular reproduce the experimentally observed isomerization states.[12]

In the present article we analyze the spectrum of DCP using this new PES. Because of the drastic change of one of the atomic masses, the DCP spectrum is completely different from the HCP level spectrum.[15] Instead of the CP stretch:bend resonance, a 2:1 DC stretch:CP stretch resonance governs the DCP spectrum. Furthermore, the bifurcations occurring in DCP are of different types than observed for HCP. Unfortunately there are no experimental results, except for the lowest levels, to compare the theoretical predictions with.

The article is organized in the following way: In Sec. II details of the numerical calculations will be briefly described. The quantum-mechanical results and the development of the polyad structure from low to high energies are investigated in Sec. III. Additional clues of the quantum-mechanical eigenvalue spectrum are provided by an analysis of the classical phase-space structure and an effective Hamiltonian model, which will be presented in Secs. IV and V, respectively. The pure bending states are briefly discussed in Sec. VI. All calculations, except where otherwise stated, are performed for nonrotating DCP ($J=0$). Energies are measured with respect to the potential minimum for linear DCP.

a)Electronic mail: rschink@gwdg.de

TABLE I. Comparison of calculated and measured transition energies ΔE and rotational constants B (in cm^{-1}) for DCP.

	ΔE		B	
(v_1,v_2^l,v_3)	Theory	Experiment[a]	Theory	Experiment
$(0,0^0,0)$	0	0	0.567	0.572
$(0,1^1,0)$	525.8	525.22	⋯	⋯
$(0,2^0,0)$	1037.2	1037.50	0.574	0.569
$(0,2^2,0)$	1053.5	1052.93	⋯	⋯
$(0,0^0,1)$	1228.7	1231.40	0.569	0.564
$(1,0^0,0)$	2419.5	2419.43	0.570	0.563
$(1,1^1,0)$	2937.5	2935.64	⋯	⋯
$(2,0^0,0)$	4790.2	4789.05	0.570	0.559
$(1,0^0,2)$	4837.0	4832.275	0.567	0.557

[a]References 18 and 20.

II. CALCULATIONS

A. Numerical details

We have performed quantum-mechanical variational calculations for determining the vibrational energies as well as the corresponding wave functions. The coordinates used are the Jacobi coordinates R (the distance between the center-of-mass of CP and D), r (the CP separation), and γ (the angle between the two vectors **R** and **r** with $\gamma=180°$ corresponding to linear DCP). The Hamiltonian is represented in a highly contracted–truncated (three-dimensional) 3D basis as described in detail in Ref. 16. The variational program requires basically two parameters: The energy E_{cut} up to which all internally contracted basis functions are included and the maximal distance in the dissociation coordinate, R_{max}. All other parameters are chosen automatically. The results reported below are obtained with $E_{\mathrm{cut}}=4.536$ eV and $R_{\mathrm{max}}=6.36a_0$. The size of the primary direct-product basis for these parameters is 322 770, whereas the dimension of the contracted–truncated basis is only 12 087. In order to assess the accuracy of the variational calculations we performed additional calculations for $E_{\mathrm{cut}}=4.486$ and 4.636 eV. The convergence is best for the pure bending states and less satisfactory for the pure CP stretch progression. The uncertainties for the energies of the CP stretch progression are estimated to be 0.1, 3, and 14 cm^{-1} for the first 100, 500, and 1000 states, respectively, which corresponds to 4, 8, and 10 quanta of the DC stretch coordinate. Most states are significantly better converged; the average error is more than one order of magnitude smaller. The qualitative behavior of the wave functions is the same for all three calculations and, therefore, we are confident that the main conclusions of the present work are not affected by convergence problems.

In order to determine the rotational constants for some of the lowest levels we also performed calculations for $J=1$ as described in Ref. 14.

B. Comparison with experimental data

Unlike HCP, the experimental information on the vibration–rotation spectrum of DCP is sparse (see Ref. 17 and references therein). Merely the transition energies of the lowest states are known.[18–20] In Table I we compare the calculated term values and rotational constants with the measured data. In what follows, ν_1 and ν_3 are the DC stretch and the CP stretch mode, respectively, and ν_2^l is the bending mode with l indicating the vibrational angular momentum quantum number. (The real meaning of these assignments, especially at higher energies, will be discussed in the next section.) The agreement between the measured and the calculated energies is excellent. It must be underlined, that the originally calculated PES had been modified very slightly in order to compensate an underestimation of the CP stretching frequency by 16 cm^{-1} in HCP.[12,14] The corresponding scaling factor was not adjusted to minimize the error for the fundamental, rather it was chosen so that good overall agreement over a large energy region was obtained.

In view of the excellent agreement for many energy levels of HCP[14] and the agreement seen in Table I for DCP, we are confident that the calculated DCP levels are well suited for guiding future SEP studies at higher excitation energies. The energies of the first hundred levels including their assignments are listed in Table II. The data for the lowest thousand states are available electronically.[21]

III. QUANTUM MECHANICAL SPECTRUM, WAVE FUNCTIONS, AND ASSIGNMENTS

We have visually inspected the lowest five hundred vibrational wave functions in order to achieve an unambiguous assignment and to elucidate how the spectrum develops with increasing energy. Above state No. 500 only selected progressions have been followed to higher energies.

A. Polyad structure for $v_2=0$

The spectrum of DCP is governed by a 2:1 anharmonic resonance between modes ν_1 and ν_3[20,22] [$E_{(0,0,2)}-E_{(1,0,0)}=41.5$ cm^{-1}]. As a result, it is structured in terms of polyads[23] [$[v_2,P]$] with ''polyad quantum number'' $P=2v_1+v_3$. The bending degree of freedom is—at least in the low and intermediate energy regimes—relatively weakly coupled to the two stretching degrees of freedom and merely plays the role of a ''spectator.'' We will first consider the spectrum for $v_2=0$; changes of the general structure with $v_2>0$ will be discussed below.

In Fig. 1(a) we show the energy spectrum for $v_2=0$ for polyad quantum numbers $P=8$–16. While the lower polyads are well separated, starting with $P=15$ the polyads overlap, which makes the assignment more and more cumbersome. All wave functions belonging to polyads [[0,6]]–[[0,9]] are depicted in Fig. 2. With a few exceptions, to be discussed below, the assignment in terms of quantum numbers v_1 and v_3 is straightforward. The quantum number v_1 counts the number of nodes along the ''left'' and ''right'' side lines of the wave function and v_3 counts the number of nodes along the lower ''arc'' [see, for example, wave function (2,0,4)]. It should be underlined that v_3 must be enumerated at the ''outer'' line of nodes, as explicitly indicated in the figure, because the number counted along the ''inner'' line may be smaller. This occurs particularly at higher excitations. As we will show below, the curves along which the number of nodes are counted correspond to particular periodic orbits in the classical phase space. The curvature of the $(0,0,v_3)$ wave functions is a result of the strong mixing between the two stretching degrees of freedom; it increases with increasing

TABLE II. Energies and assignments of the first 100 states of DCP.

No.	(v_1,v_2,v_3)	E [eV]	ΔE [cm^{-1}]	No.	(v_1,v_2,v_3)	E [eV]	ΔE [cm^{-1}]
1	0 0 0	0.295 17	0.00	51	1 0 4	1.193 15	7242.58
2	0 2 0	0.423 76	1037.17	52	1 10 0	1.204 80	7336.60
3	0 0 1	0.447 51	1228.68	53	0 0 6	1.207 13	7355.37
4	0 4 0	0.549 99	2055.22	54	0 10 2	1.218 73	7448.89
5	0 2 1	0.576 18	2266.51	55	1 8 1	1.236 30	7590.60
6	1 0 0	0.595 15	2419.44	56	0 8 3	1.250 22	7702.94
7	0 0 2	0.600 29	2460.91	57	2 6 0	1.252 70	7722.91
8	0 6 0	0.674 17	3056.84	58	1 6 2	1.266 33	7832.85
9	0 4 1	0.702 16	3282.52	59	0 16 0	1.268 84	7853.09
10	1 2 0	0.721 54	3438.88	60	0 6 4	1.280 05	7943.52
11	0 2 2	0.728 67	3496.34	61	2 4 1	1.282 66	7964.54
12	1 0 1	0.745 13	3629.13	62	1 4 3	1.294 04	8056.36
13	0 0 3	0.752 70	3690.16	63	3 2 0	1.297 41	8083.55
14	0 8 0	0.796 48	4043.29	64	0 14 1	1.302 68	8125.98
15	0 6 1	0.825 96	4281.09	65	0 4 5	1.308 09	8169.64
16	1 4 0	0.845 12	4435.61	66	2 2 2	1.309 56	8181.50
17	0 4 2	0.854 27	4509.36	67	1 2 4	1.319 41	8260.91
18	1 2 1	0.871 84	4651.11	68	1 12 0	1.321 36	8276.65
19	0 2 3	0.880 83	4723.62	69	3 0 1	1.323 52	8294.06
20	2 0 0	0.889 08	4790.13	70	2 0 3	1.330 44	8349.91
21	1 0 2	0.894 88	4836.93	71	0 2 6	1.334 63	8383.68
22	0 0 4	0.904 69	4916.08	72	0 12 2	1.336 44	8398.31
23	0 10 0	0.917 02	5015.51	73	1 0 5	1.341 59	8439.88
24	0 8 1	0.947 81	5263.82	74	1 10 1	1.354 03	8540.22
25	1 6 0	0.966 72	5416.34	75	0 0 7	1.357 44	8567.70
26	0 6 2	0.977 71	5505.03	76	0 10 3	1.369 24	8662.81
27	1 4 1	0.995 39	5647.62	77	2 8 0	1.370 23	8670.81
28	0 4 3	1.006 05	5733.56	78	0 18 0	1.382 92	8773.22
29	2 2 0	1.012 91	5788.88	79	1 8 2	1.385 62	8794.97
30	1 2 2	1.021 64	5859.34	80	0 8 4	1.400 47	8914.74
31	0 2 4	1.032 58	5947.53	81	2 6 1	1.401 69	8924.61
32	0 12 0	1.035 89	5974.28	82	1 6 3	1.414 87	9030.88
33	2 0 1	1.037 39	5986.32	83	3 4 0	1.415 74	9037.86
34	1 0 3	1.044 21	6041.32	84	0 16 1	1.417 70	9053.70
35	0 0 5	1.056 19	6138.00	85	0 6 5	1.429 80	9151.30
36	0 10 1	1.067 80	6231.64	86	2 4 2	1.431 16	9162.27
37	1 8 0	1.086 59	6383.19	87	1 14 0	1.436 26	9203.40
38	0 8 2	1.099 18	6484.72	88	1 4 4	1.442 21	9251.36
39	1 6 1	1.116 78	6626.62	89	3 2 1	1.445 26	9275.97
40	0 6 3	1.129 14	6726.35	90	0 14 2	1.452 44	9333.93
41	2 4 0	1.133 71	6763.20	91	2 2 3	1.455 48	9358.41
42	1 4 2	1.145 10	6855.10	92	4 0 0	1.456 13	9363.69
43	0 14 0	1.153 16	6920.07	93	0 4 6	1.458 70	9384.40
44	0 4 4	1.157 39	6954.19	94	1 2 5	1.467 34	9454.09
45	2 2 1	1.161 74	6989.30	95	3 0 2	1.469 10	9468.28
46	1 2 3	1.170 81	7062.40	96	1 12 1	1.470 04	9475.84
47	3 0 0	1.176 14	7105.38	97	2 0 4	1.476 09	9524.65
48	0 2 5	1.183 71	7166.48	98	0 2 7	1.484 70	9594.06
49	2 0 2	1.184 62	7173.77	99	2 10 0	1.485 81	9603.04
50	0 12 1	1.186 06	7185.44	100	0 12 3	1.486 70	9610.18

quantum number v_3. The overtones $(v_1,0,0)$ are always at the bottom of the polyad and the states $(0,0,v_3)$ mark the top of a polyad. This ordering was different for the old PES.[15] Combination states like (1,0,5), (1,0,7), or (2,0,5) can be easily identified. The $(v_1,0,0)$ wave functions retain their general shape up to high energies; their main character is excitation of the DC stretch bond distance and therefore it is reasonable to term them DC stretching states. The $(0,0,v_3)$ states also preserve their general structure as v_3 increases, only the ''curvature'' in the (R,r)-plane becomes more pronounced. Already the lowest member of this progression, $(0,0,1)$, shows excitations of both the DC and the CP bond, so that a classification as CP stretching states is misleading.

Most states up to $P=20$ or so can be assigned as described in Fig. 2. However, there exist a few states, which do not clearly fall into the two classes $(v_1,0,0)$ and $(0,0,v_3)$ or combinations of them, but which form a different class. The states $(v_1,0,v_1)$ with $v_1=3,4,\ldots$ $(P=9,12,\ldots)$ are the clearest examples (middle column of Fig. 3). They gradually develop a new type of shape with increasing v_1. Their ''backbone'' is strongly curved in the (R,r)-plane, too, but in the opposite direction than observed for the $(0,0,v_3)$ states. While the assignment (3,0,3) for the second lowest state in polyad $P=9$ is still meaningful, as plotting of the

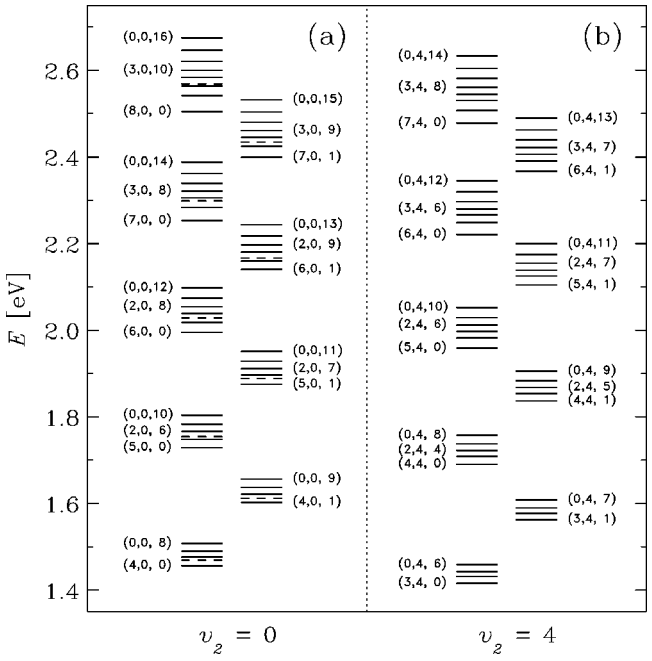

FIG. 1. Energy-level spectrum for (a) $v_2=0$ and (b) $v_2=4$. The special states $(0,0,v_3)_r$ for $v_2=0$ are indicated by dashed lines [(3,0,2), (3,0,3), (3,0,4), etc.]. Energy is measured with respect to the minimum of the PES.

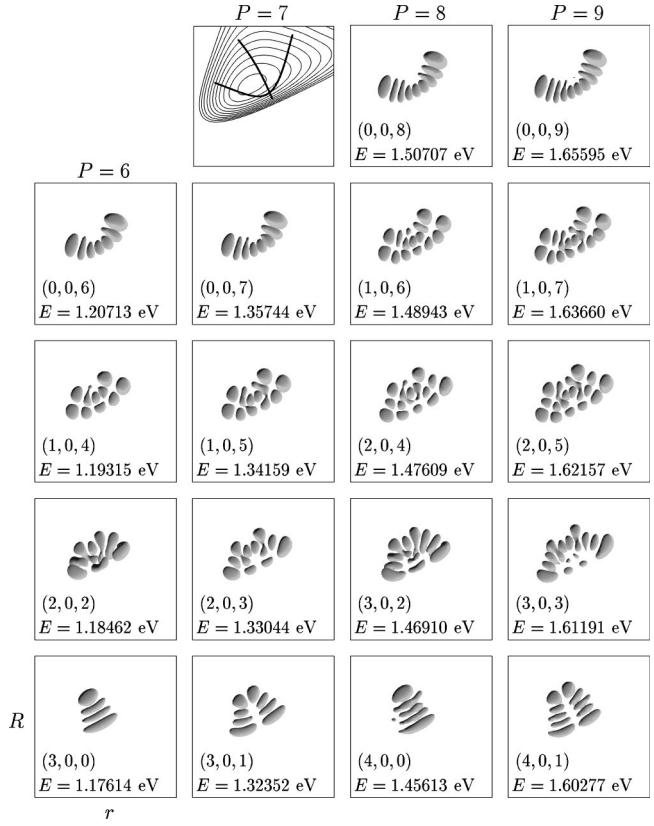

FIG. 2. All wave functions in polyads [[0,6]]–[[0,9]]. All wave function plots depicted in this article, if not stated otherwise, have been obtained from a plotting routine, which allows to rotate 3D objects in space. Shown is one particular contour $\epsilon(R,r,\gamma)=\sin\gamma|\Psi(R,r,\gamma)|^2$ with the value of ϵ being the same in a particular figure. The plots are viewed along one coordinate axis, in the direction perpendicular to the plane of the other two coordinates. Shading emphasizes the 3D character of the wave functions. The top panel in the second column shows the potential energy surface and representative periodic orbits of the $[R]$ (mainly R motion) and the $[R1]$ (motion along both R and r) families. The R axis ranges from $2.20a_0$ to $5.50a_0$ and the r axis ranges from $2.20a_0$ to $3.90a_0$.

wave function with a lower contour level shows, interpretation of the wave function shown for $P=18$ as (6,0,6) does not make sense. The assignments (5,0,5), (6,0,6) etc., reflect the positions of these states in the spectrum rather than the shapes of their wave functions. The classical analysis of the phase space indicates that these particular states are related to a class of periodic orbits, which essentially describe motion in the CP stretch coordinate r (see Sec. IV), and therefore, we will alternatively assign them as $(0,0,v_3)_r$ in order to distinguish them from the $(0,0,v_3)$ states. The number of nodes along the backbones of the $(0,0,v_3)_r$ wave functions is identical with P.

States of the form $(v_1,0,v_1)$ exist only for polyad quantum numbers, which are multiples of 3. Wave functions with the character of the $(0,0,v_3)_r$ states do exist also for the other polyads, however, then v_1 and v_3 must differ by one, i.e., $v_1-v_3=\pm 1$ (see the first and third columns in Fig. 3). However, at comparable energies these states have a less pronounced $(0,0,v_3)_r$ character than the states with $v_1=v_3$.

In order to illustrate the variations of wave functions within a complete polyad, we depict in Fig. 4 the wave functions of all states belonging to [[0,18]], one of the highest polyads, that has been completely assigned. With increasing energy the intra- and inter-polyad coupling steadily increases with the result that more and more wave functions are strongly mixed, for example (8,0,2).

It is astounding, that not the states $(0,0,v_3)_r$ but the $(0,0,v_3)$ levels are the counterparts of the DC stretching states $(v_1,0,0)$. The $(0,0,v_3)_r$ wave functions have strong excitation in r and relatively little excitation in R and, therefore, they do complement the $(v_1,0,0)$ states, which show strong excitation in R and only slight displacements in r. In contrast, the $(0,0,v_3)$ wave functions have relatively strong excitation in *both* R and r. It is also astonishing that the $(0,0,v_3)_r$ states become pronounced only in the higher polyads, while they are not clearly discernible in the lower polyads. The semiclassical analysis of an effective Hamiltonian will provide explanations for these riddles (Sec. V).

Actually, careful inspection of the wave functions reveals that the wave functions like (2,0,2), (3,0,3) (Fig. 2) or (3,0,4) (Fig. 3) are mixtures of the $(0,0,v_3)$ and the $(0,0,v_3)_r$ wave functions. For example, (4,0,5) in Fig. 3 is clearly a mixture of $(0,0,13)_r$ and (4,0,5) and similarly (5,0,6) is a superposition of wave functions $(0,0,16)_r$ and (5,0,6) as a blow-up of the wave functions undoubtedly shows. Thus, the $(0,0,v_3)_r$ wave functions do exist in the low-energy part of the spectrum, but they are interwoven with the $(0,0,v_3)$ wave functions and therefore obscured. The degree of this mixing seems to decrease with increasing energy, so that the $(0,0,v_3)_r$ character becomes more distinct. The wave function for state $(0,0,18)_r$ is the best example in Fig. 3.

This qualitative behavior may become understandable in terms of the energy dependent transition frequencies, i.e., energy differences between adjacent levels, of the three progressions $(v_1,0,0)$, $(0,0,v_3)$, and $(0,0,v_3)_r$, respectively

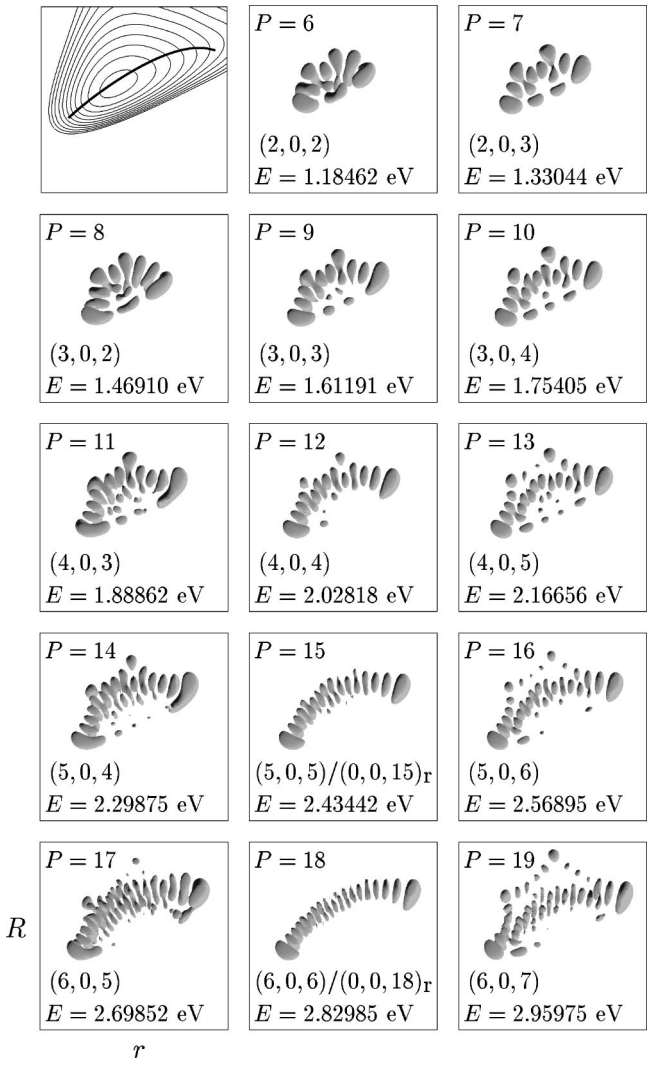

FIG. 3. Wave functions of states $(v_1,0,v_1)$, etc. See the text for more details. The first panel shows the potential energy surface and a representative periodic orbit of the $[r]$ family. The R axis ranges from $2.20a_0$ to $5.50a_0$ and the r axis ranges from $2.20a_0$ to $3.90a_0$. See Fig. 2 for more details.

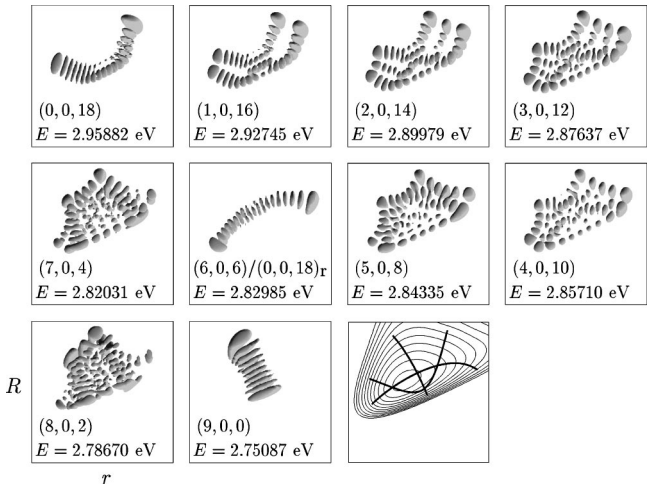

FIG. 4. All wave functions of polyad [[0,18]]. See Figs. 2 and 3 for more details.

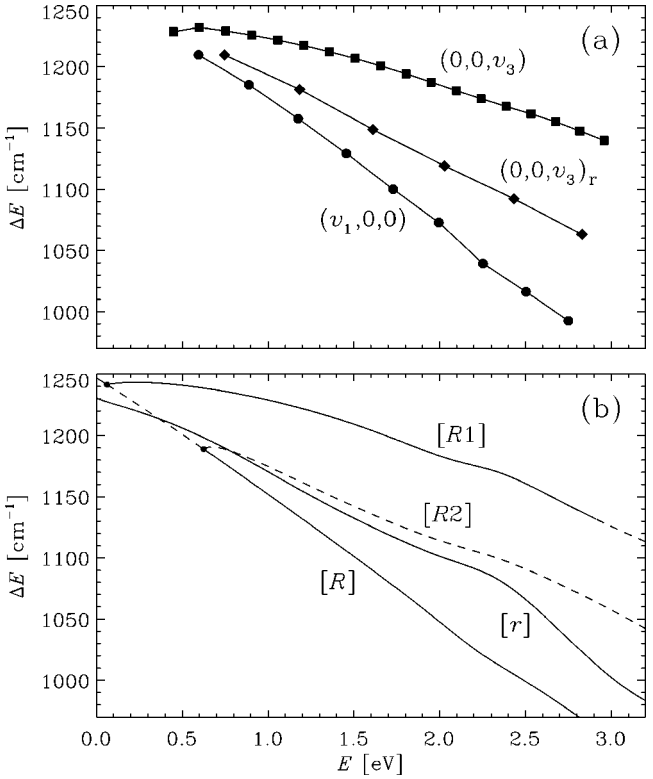

FIG. 5. (a) Transition energies, i.e., energy differences between neighboring levels, for the three progressions $(v_1,0,0)$ (divided by 2), $(0,0,v_3)$, and $(0,0,v_3)_r$ (divided by 3). Each symbol is plotted at the energy of the upper state. (b) Frequencies of the periodic orbits of the families $[R]$ (divided by 2), $[R1]$, $[R2]$, and $[r]$. Stable (unstable) branches are indicated by solid (dashed) curves. The two dots mark the bifurcations discussed in the text.

$(v_1,0,v_1)$ depicted in Fig. 5(a). The energies for the $(v_1,0,0)$ progression are divided by 2 because of the 2:1 resonance and the energies of the $(0,0,v_3)_r$ progression are divided by 3, because there is only one entry for every third polyad. The transition frequency for the bending mode is considerably smaller (1037 cm^{-1} for the lowest transition) and not shown in Fig. 5(a).

At low energies, the transition frequencies for all three progressions are very close together, which implies that here the mixing of modes is strongest. Due to the different anharmonicities of the three progressions, the gap between the transition energies widens. This means that the energy range, over which a polyad spreads, increases with energy (Fig. 1), which in turn may explain, why the mixing between the states $(0,0,v_3)$ and $(0,0,v_3)_r$ gradually diminishes in the higher polyads. In this respect, there is one detail worth mentioning: The transition energy of the $(0,0,v_3)$ progression first *increases* with v_3 rather than decreases as expected for a vibrational progression. This indicates that the (0,0,1) state is not a true member of the $(0,0,v_3)$ progression and the wave function (not shown here) actually confirms this. The (0,0,1) wave function fits better into the $(0,0,v_3)_r$ progression, rather than the $(0,0,v_1)$ series.

It is interesting to compare Fig. 5 with the equivalent plots for HCP [Fig. 9(a) in Ref. 12] and HOCl [Fig. 5(c) in Ref. 24], another system which is characterized by a 1:2 resonance. In HCP the gap between the two relevant transi-

tion energies remains almost constant over a large energy interval and therefore the degree of mixing does not change much. For HOCl, on the other hand, the difference between the transition energies is relatively large at low energies but decreases with E, because one mode has a significantly larger anharmonicity than the other mode. As a consequence, with increasing excitation the system is gradually tuned into the resonance.

Since the $(0,0,v_3)_r$ states do not naturally fit into the $(v_1,0,P-2v_1)$ level scheme, it is not surprising to find, that their energies lead to some ''distortions'' in the intra-polyad energy spacing, that is the energy spacing Δ_i between neighboring levels inside a particular polyad. This is clearly seen in Fig. 1, where the levels of the $(0,0,v_3)_r$ states are indicated by dashed lines. Plotting Δ_i as a function of the index i shows clear minima, which are caused by the $(0,0,v_3)_r$ states. The ''dips'' are associated with a separatrix caused by a particular unstable periodic orbit (see Sec. V).

B. Polyad structure for $v_2=2$ and 4

Because the bending mode is more or less decoupled from the other two degrees of freedom, the general structure in terms of polyads is essentially preserved for $v_2>0$. However, the separation is not perfect and therefore differences between the spectra for $v_2=0$ and $v_2\neq 0$ do exist. This is exemplified in Fig. 1(b), where the spectrum for $v_2=4$ is compared with the $v_2=0$ spectrum. The energetic breadth of comparable polyads is slightly larger for $v_2=4$. More important, however, the spacings inside the polyads is noticeably different for $v_2=0$ and 4, pointing towards a different dynamics.

The wave functions for $v_2=2$ and 4 look quite similar to the $v_2=0$ wave functions, except for the additional nodes in the bending coordinate. (Figures equivalent to Figs. 2 and 3 but for $v_2=2$ and 4 are available electronically.[21]) The assignments with quantum numbers v_1 and v_3 is analogous as described above. However, the special states $(0,0,v_3)_r$ play a minor role as compared to $v_2=0$; they start at higher polyads and are less pronounced. For example, for $v_2=2$ the first indication of a $(0,0,v_3)_r$ state occurs at $P=13$ and the first clear-cut example appears at $P=16$. For $v_2=4$ there are no distinct $(0,0,v_3)_r$ wave functions up to $P=16$. These observations are in good qualitative accord with the semiclassical analysis of the resonance Hamiltonian in Sec. V. At higher energies, the wave functions become more and more complicated and unique assignments are generally difficult, except for special cases. The spectra for still higher bending quantum numbers have not been analyzed in detail, but the semiclassical analysis predicts them to be similar to the $v_2=4$ spectra.

The minor peculiarity of the $(0,v_2,v_3)_r$ states leads to a more gradual energy spacing between neighboring levels in a particular polyad as is clearly seen in Fig. 1(b) for $v_2=4$ as compared to $v_2=0$. Δ_i does show a minimum vs i; however, this minimum is less pronounced than for $v_2=0$. Thus, although the bending degree of freedom is only weakly coupled to the other two modes, the spectra for different values of v_2 exhibit noticeable differences.

IV. ANALYSIS OF CLASSICAL PHASE SPACE

The structure of the quantum-mechanical spectrum and particularly the shapes of the wave functions can be elucidated in terms of the structure of the classical phase space and special trajectories therein, so-called periodic orbits (POs).[25,26] POs are classified as stable or unstable depending on the eigenvalues of the monodromy matrix.[8] For many systems it has been demonstrated that the backbones of quantum-mechanical wave functions closely follow certain stable POs.[27] DCP is a particularly illuminating system for illustrating the close correspondence between the phase-space structure and the quantum-mechanical spectrum, all the way from the bottom of the potential well up to high energies.

Near the bottom of the potential well there are three types of stable POs, the so-called principal families. They are denoted by $[R]$, $[r]$, and $[\gamma]$, respectively, because the corresponding POs basically describe motions along the three coordinate axes. Instead of showing individual POs we present in Fig. 5(b) the corresponding frequencies as functions of the energy (continuation–bifurcation diagram[28,29]). In order to simplify the presentation, the frequency for the $[\gamma]$ family is not shown. In accordance with the quantum-mechanical results in Fig. 5(a) the frequencies of the $[R]$-type orbits are divided by two. The trajectories of the $[R]$ and $[r]$ families (as well as the $[R1]$ and $[R2]$ manifolds discussed below) lie in the (R,r)-plane, i.e., $\gamma=180°$.

Despite the simplicity of the PES around the equilibrium, the structure of the classical phase space is already quite involved even at very low energies. The $[R]$-type POs become unstable in a period-doubling bifurcation already at an energy of 0.061 eV. At the same time a new class of POs, termed $[R1]$ in what follows, is born; the corresponding orbits are stable. Shortly after the first bifurcation, the $[R]$-type POs become stable again in a second period doubling bifurcation ($E=0.626$ eV), in which another class of orbits, $[R2]$, is created. The $[R2]$ orbits are unstable and do not influence the quantum wave functions. After the second bifurcation the $[R]$ trajectories remain stable up to high energies. The $[R1]$ POs remain stable until a third bifurcation at $E=2.920$ eV destabilizes them. The $[r]$-type POs are stable from low to very high energies. Incidentally we note, that the bifurcation of the $[R]$ family, at which the stable $[R1]$ orbits are born, is also predicted by the old HCP PES, however, at significantly higher energies.[15] As a consequence of this rather late appearance of the $[R1]$ trajectories the corresponding spectrum is remarkably different from the spectrum discussed in the present work.

The classical continuation–bifurcation diagram looks qualitatively very similar to the quantum-mechanical transition energies. A direct comparison is not quite straightforward, because of the different ways in which the various curves are plotted in Figs. 5(a) and 5(b). In the quantum-mechanical representation each point corresponds to the energy of the upper level, whereas in the classical picture the nominal energy is the total energy of the trajectories. A quantitative comparison must also include modifications in order to correct for zero-point energies, which has not been done. Nevertheless, the good qualitative agreement suggests

that the states $(v_1,0,0)$, $(0,0,v_3)$, and $(0,0,v_3)_r$ correspond to the POs of the $[R]$, $[R1]$, and $[r]$ families, respectively. This correspondence is also confirmed by the POs and their scarring of the complementary wave functions. In Fig. 2 we depict POs for the $[R]$ and $[R1]$ families and even without overlaying them to the wave functions it is clear that they guide the $(v_1,0,0)$ and $(0,0,v_3)$ wave functions, respectively. Likewise, in Fig. 3 we show POs of the $[r]$ type and it is obvious that they scar the $(0,0,v_3)_r$ wave functions.

A question, which we do not have an answer for within the classical framework, is, why quantum mechanics follows predominately the $[R1]$ branch rather than the $[r]$ branch of POs. The $[r]$-type POs belong to a principal family and they are stable. In other words, there is no obvious reason, why the wave functions should not follow them. Wave functions with clear-cut CP stretch behavior come into existence only at higher energies. An explanation is provided by the semiclassical analysis of the effective Hamiltonian model described in the next section.

V. EFFECTIVE HAMILTONIAN MODEL

More details and more insight into the dynamics comes from a model, which is very simple, but which nevertheless reproduces the quantum-mechanical level spectrum and the wave functions remarkably well. The main asset of this model is the possibility of a semiclassical analysis, which would be very difficult for the exact classical Hamiltonian. Similar studies have been recently performed for HCP[12,30,31] and HOCl[32] so that only a few details of the actual calculations are reported here. The interested reader is referred to Refs. 30–32 for more explanations.

The starting point is the observation that a simple Dunham expansion [Eq. (2) below] is unable to correctly reproduce the quantum-mechanical spectrum, whereas this is possible when a more refined model is used, which takes into account the 2:1 Fermi resonance between the DC stretch and the CP stretch modes. More precisely, the Fermi resonance Hamiltonian is written as

$$H = H_D + H_F. \tag{1}$$

The Dunham part is defined as

$$\langle v_1,v_2,v_3|H_D|v_1,v_2,v_3\rangle = \sum_i \omega_i n_i + \sum_{i\leqslant j} x_{ij} n_i n_j + \sum_{i\leqslant j\leqslant k} y_{ijk} n_i n_j n_k + \sum_{i\leqslant j\leqslant k\leqslant m} z_{ijkm} n_i n_j n_k n_m, \tag{2}$$

with $n_1 = v_1 + \frac{1}{2}$, $n_2 = v_2 + 1$, and $n_3 = v_3 + \frac{1}{2}$ and the Fermi off-diagonal term is given by

$$\langle v_1,v_2,v_3|H_F|v_1-1,v_2,v_3+2\rangle = [v_1(v_3+1)(v_3+2)]^{1/2}\left(k + \sum_i \lambda_i n_i + \sum_{i\leqslant j} \mu_{ij} n_i n_j\right), \tag{3}$$

TABLE III. Parameters of the effective Hamiltonian model.

Parameter	Value	Standard deviation	Parameter	Value	Standard deviation
ω_1	2494.0412	3.7552	y_{223}	−0.0482	0.0080
ω_2	539.1611	0.5725	y_{233}	0.2535	0.0564
ω_3	1237.0955	1.7274	y_{333}	−0.2447	0.0490
x_{11}	−24.0769	1.7791	z_{1111}	0.0510	0.0149
x_{12}	−11.1041	0.2866	z_{1112}	0.0806	0.0105
x_{13}	−4.6276	0.6920	z_{1222}	−0.0055	0.0005
x_{22}	−3.5142	0.0825	z_{1233}	0.0280	0.0086
x_{23}	−0.6753	0.2721	z_{2222}	−0.0014	0.0001
x_{33}	−2.2082	0.5279	z_{2233}	−0.0067	0.0012
y_{111}	−0.8896	0.2913	z_{2333}	−0.0132	0.0026
y_{112}	−0.4928	0.0906	z_{3333}	0.0092	0.0014
y_{113}	−0.5407	0.0734	k	12.3422	0.1690
y_{122}	0.2167	0.0175	λ_1	0.5786	0.1363
y_{123}	−0.3655	0.0505	λ_3	0.1212	0.0157
y_{133}	−0.2167	0.0470	μ_{11}	−0.2990	0.0252
y_{222}	0.0884	0.0040			

with $n_1 = v_1$, $n_2 = v_2 + 1$, and $n_3 = v_3 + \frac{3}{2}$. Since only $J = 0$ states are investigated, the vibrational angular momentum constant is zero (and therefore omitted) in Eqs. (2) and (3). The Fermi resonance Hamiltonian has two conserved quantities, i.e., the number of quanta in the bending degree of freedom, v_2, and the polyad quantum number, P.

The constants ω_i, x_{ij}, y_{ijk}, z_{ijkm}, k, λ_i, and μ_{ij} can be obtained either from high-order canonical perturbation theory, as was done in Ref. 33, or from a fit of the quantum-mechanical energy levels, as was done in Refs. 23, 31, and 32 as well as in the present study. A total of 533 assigned levels are taken into account in the fitting procedure. They include all levels up to No. 481 (17 292 cm^{-1} above the ground state, corresponding up to 38 quanta in the bending degree of freedom) and all additional levels with $v_2 = 0$ up to No. 996 (21 922 cm^{-1} above the ground state, corresponding up to 20 quanta in the CP stretch). The 533 transition energies are reproduced with a rms (root-mean-square) error of 4.26 cm^{-1} and a maximum error of 24.71 cm^{-1} using a set of 31 parameters, which are listed in Table III together with their standard deviations. Most important, however, is the fact, that the resonance Hamiltonian, in addition to the energy values, also reproduces satisfactorily the exact quantum wave functions, as can be seen by comparing the approximate ones for polyad [[0,18]] in Fig. 6 with those in Fig. 4. The tilting of the coordinate axes between the two representations reflects the nonlinear relationship between the Jacobi coordinates (R,r) used in the exact calculations and the (abstract) normal coordinates (q_1,q_3) employed in the model Hamiltonian. The approximate wave functions have a built-in symmetry, which is not present in the exact Hamiltonian. Also, interpolyad coupling is not accounted for by the effective Hamiltonian. Nevertheless, the generic structures of the wave functions are accurately described. In particular, the peculiar behavior of the wave function for level No. 797—$(0,0,18)_r$ in the terminology used above—is clearly reproduced.

The classical counterpart for the quantum Hamiltonian in Eqs. (1)–(3) is given by

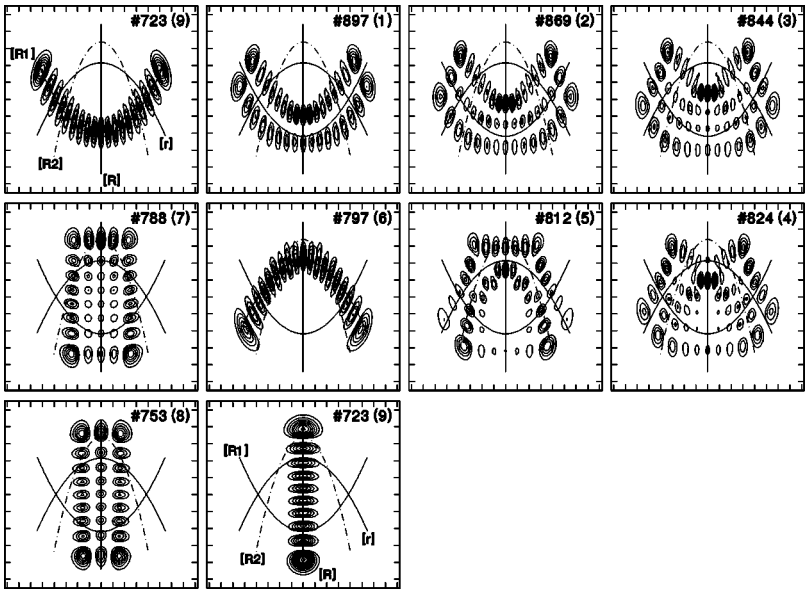

FIG. 6. Two-dimensional contour plots of the approximate wave functions for polyad [[0,18]] as obtained from the resonance Hamiltonian. The number in each panel indicates the number in the complete spectrum and the number in bracket indicates the ordering inside the polyad ($i=0$ for the highest level). The curves represent the corresponding periodic orbits for the various families as indicated.

$$H_{\rm cl}=\sum_i \omega_i I_i+\sum_{i\leqslant j} x_{ij}I_iI_j+\sum_{i\leqslant j\leqslant k} y_{ijk}I_iI_jI_k + \sum_{i\leqslant j\leqslant k\leqslant m} z_{ijkm}I_iI_jI_kI_m+2I_1^{1/2}I_3\cos(\varphi_1-2\varphi_3) \times\left(k+\sum_i \lambda_i I_i+\sum_{i\leqslant j}\mu_{ij}I_iI_j\right), \quad (4)$$

where the I_i and φ_i are the zero-order action-angle variables of the ith normal mode. Using the new coordinates

$$I=2I_1+I_3, \quad J=2I_1, \quad \Theta=\varphi_3, \quad \psi=\frac{\varphi_1}{2}-\varphi_3, \quad (5)$$

where Θ is conjugate to I and ψ is conjugate to J, $H_{\rm cl}$ is seen to depend on a single angle, namely ψ. As a consequence, I_2 and I are constants of motion. When the total energy E, I, and I_2 are fixed, it follows that J is a function of ψ only and one can define the quantity

$$\mathcal{J}=\frac{1}{2\pi}\oint_{\psi\in[0,\pi]} J\,d\psi. \quad (6)$$

The Einstein–Brillouin–Keller (EBK) semiclassical quantization rules[34] state, that each quantum state is associated with a unique classical trajectory (called the ''quantizing'' trajectory), so that

$$I_2=v_2+1, \quad I=P+\tfrac{3}{2}, \quad (7)$$

and $\mathcal{J}=\pm 1/2,\pm 3/2$, etc. The advantage of studying the approximate classical resonance Hamiltonian rests on the possibility to discuss POs in a four-dimensional phase space as functions of the conserved quantities I_2 and I (or alternatively the quantum numbers v_2 and P) rather than in the full six-dimensional phase space as done in Sec. IV. This provides a more detailed picture.

The classical results reported in Sec. IV are retrieved by seeking the POs for $I_2=0$, that is $v_2=-1$; in these calculations no energy is put into the bending degree of freedom. Just above the zero-energy point (ZEP) one finds two families of stable POs with the same DC and CP stretching characteristics as described in Sec. IV and which are, therefore, termed $[R]$ and $[r]$, respectively. A first bifurcation occurs at $P=-1.29$ corresponding to an energy of 261 cm^{-1} above the ZEP. This period-doubling bifurcation is a *pitchfork* bifurcation in the terminology of elementary bifurcations.[35,36] At this first bifurcation, PF1, the $[R]$-type POs become unstable and the family of stable $[R1]$ POs is created. At $P=2.96$, corresponding to 5437 cm^{-1} above the ZEP, a second pitchfork bifurcation, PF2, occurs, where the $[R]$-type POs become stable again while a family of unstable POs, $[R2]$, is created. These results are in very good agreement with the full classical results obtained from the original PES, which lead to bifurcations at 494 and 5049 cm^{-1} above the potential minimum.

According to the semiclassical quantization rules in Eq. (7), the study of the polyads for a fixed bending quantum number $v_2=0$ requires examination of the POs with $I_2=1$ instead of $I_2=0$ as done above. The general behavior of the bifurcation diagram is found to be very similar to the classical case for $I_2=0$, that is, the family of stable POs, $[R1]$, is created in a first pitchfork bifurcation PF1 at $P=-1.43$ (620 cm^{-1} above the ZEP), while the family of unstable POs, $[R2]$, originates at a second pitchfork bifurcation PF2 at $P=2.35$ (5224 cm^{-1} above the ZEP). The inset of Fig. 7 shows the energies (with respect to the ground vibrational state) of the four different types of POs as functions of the polyad quantum number P. In order to make details more discernible, we plot in the main part of the figure the energies relative to the energy of the $[R]$-type POs. It is seen that for values of P larger than four or so the $[R]$- and $[R1]$-type POs constitute the lower and the upper bounds of the classically accessible region. This is the reason why the states close to the low- and the high-energy ends of the polyads are scarred by the $[R]$ and the $[R1]$ POs, respectively, rather than the $[r]$ trajectories. On the other hand, the $[r]$ and $[R2]$ POs remain always close to each other and their (relative)

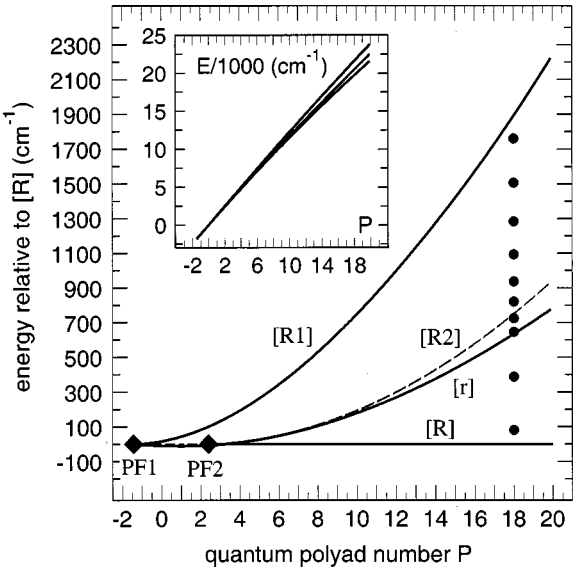

FIG. 7. The energies of the various periodic orbits as functions of the polyad number P relative to the ground-state level (inset) or relative to the energy of the $[R]$-type periodic orbit (main body of the figure). PF1 and PF2 mark the two pitchfork bifurcations. Solid lines are used for stable orbits and dashed lines for unstable ones. The filled circles indicate the energies for the states of the [[0,18]] polyad.

positions inside the classically accessible region do not vary much as P increases from about 10–20. The important point is that the quantum states, which are scarred by the $[r]$ family of POs, are expected to lie between the energies of the $[r]$ and the $[R2]$ POs. This is actually confirmed in Fig. 8, which shows the action integral $\mathcal{J}$ as a function of energy for polyad [[0,18]]. The dots indicate the positions of the quantizing trajectories which, according to the EBK quantization rules, correspond to half-integer values of $\mathcal{J}$; the number above each point indicates the position i of that particular state in the polyad as in Fig. 6 and the vertical dashed lines indicate the energies of the four POs for this polyad. Each state located on either one of the two main branches (those with negative values of $\mathcal{J}$) is seen to have a wave function

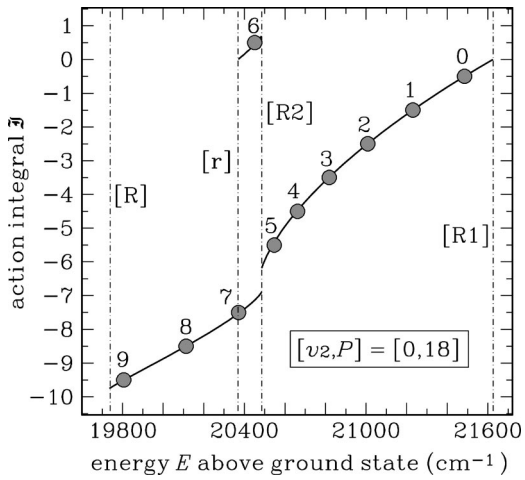

FIG. 8. Action integral $\mathcal{J}$ as function of energy for polyad [[0,18]]. The filled circles mark the quantizing periodic orbits and the vertical dashed lines denote the energies of the four periodic orbits. The numbers $i=0,1,\ldots$ indicate the ordering of the quantum levels inside the polyad.

scarred along the $[R]$ or the $[R1]$ POs; they form the main body of the polyad and are assigned as $(v_1,0,v_3)$ as described in Sec. III. State $i=6$, located on the tiny branch, which has positive values of $\mathcal{J}$ and which extends from $[r]$ to $[R2]$, is scarred along the $[r]$ orbits. It corresponds to the states termed $(0,0,v_3)_r$ above. The fact that the quantizing trajectories for the latter are comprised between the POs $[r]$ and $[R2]$ explains, why the states $(0,0,v_3)_r$ are always located approximately at the same place inside the quantum polyad. Moreover, the very slow growth of the gap between the energies of the $[r]$ and the $[R2]$ trajectories is the reason, why states scarred along the $[r]$ POs are observed only for rather large values of P and why their quantity in each polyad is so small.

At last, it should be noted that the $[R2]$ family of unstable POs is responsible for the dip in the energy gap between neighboring levels belonging to the same polyad. This phenomenon, which has been discussed in detail for HCP[11,12,30,31] and HOCl,[24] is due to the fact that the derivative of $\mathcal{J}$ with respect to energy goes to infinity at the energy of the $[R2]$ family, so that the spacing is smaller close to the energy of $[R2]$ and larger far away from it. This is clearly seen in Fig. 8. Since the branch with positive values of $\mathcal{J}$, which contains the quantizing trajectories associated with the $(0,0,v_3)_r$ states, is so narrow and contains so few states (at most one in the energy range studied), the fluctuating pattern found for HCP[31] does not occur for DCP and $[R2]$ is, therefore, associated with a simple minimum in the plot of the energy gap inside a polyad.

Let us now briefly consider the polyads with $v_2 \geqslant 2$. For these polyads, the bifurcation diagrams differ considerably from those for $v_2=0$. For $v_2=2$, the same pitchfork bifurcation PF1 as for $v_2=0$ is found, at $P=-1.45$ or 1654 cm^{-1} above the ZEP. However, the second pitchfork bifurcation, PF2, is associated with the *destruction* of the stable family of POs $[R1]$, which is born at PF1, rather than the creation of the unstable family $[R2]$. As a result, there exist only two families of stable POs up to about 16 000 cm^{-1} above the ground state, which are $[R]$ and $[r]$. Therefore, quantum wave functions are scarred by only two different POs in this energy range. Note, however, that the $[r]$-type POs for $v_2=2$ have the same structure as the $[R1]$ POs discussed for $v_2=0$. In addition, a first tangent (or saddle-node) bifurcation is found at $P=13.04$ or 16 068 cm^{-1} above the ground state, where a stable and an unstable family of POs are simultaneously created. The orbits of the stable branch have the characteristic of the $[r]$-type POs discussed for $v_2=0$ above. This is in accord with the quantum wave functions obtained from the full Hamiltonian, which show a first member of the $(0,2,v_2)_r$ progression not before $P=13$ corresponding to about 16 000 cm^{-1} above $(0,0,0)$.[21]

For $v_2=4$, pitchfork bifurcations are no longer observed and the first tangent bifurcation is found at $P=16.46$ or 20 700 cm^{-1} above the ground state. This is also in agreement with the analysis of the quantum wave functions: For $v_2=4$, up to polyad [[4,16]] (the highest member of this polyad has an energy of 20 246 cm^{-1}) clear-cut $(0,4,v_2)_r$ wave functions do not exist.[21] Polyads with values of v_2 larger than four behave as for $v_2=4$, save for the

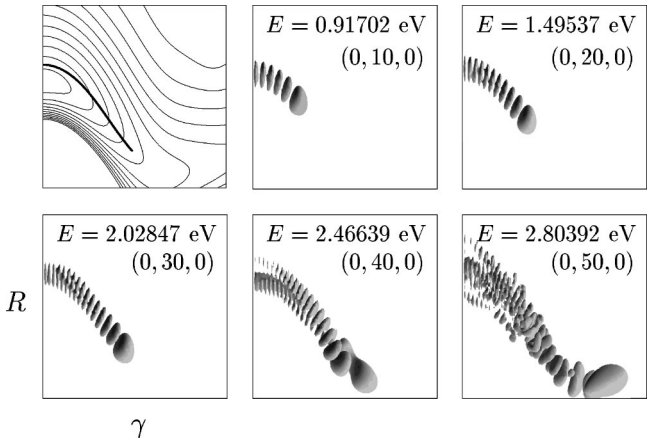

FIG. 9. Selected wave functions of the pure bending progression. The vertical axes range from $2.20a_0$ to $5.50a_0$ and the horizontal axes range from 180° to 80°. The first panel shows the potential energy surface and a representative periodic orbit of the $[B]$ family.

increase of the energy at which the first tangent bifurcation sets in with increasing v_2.

VI. PURE BENDING PROGRESSION

One of the main features in the vibrational spectrum of HCP is the strong mixing between the CP stretch mode and the bending mode due to a 1 : 2 anharmonic resonance. As a result of this mixing, the states of the $(0,v_2,0)$ progression, which at low energies have mainly the character of bending motion, gradually acquire more and more CP stretching behavior and as a consequence avoid the minimum energy path from the HCP side to the CPH side of the PES. The wave functions of all members of the $(0,v_2,0)$ progression for HCP are confined to displacements of 40°–50° away from the equilibrium angle, although larger displacements are definitely energetically accessible. States, which do follow the minimum energy path along the isomerization coordinate are born at relatively high energies in a saddle-node bifurcation.[12]

The bending dynamics in DCP is completely different. The bending mode is not involved in an anharmonic resonance with one (or both) of the other two modes, but is more or less separated. As a consequence, there is no reason for the wave functions of the bending progression *not* to evolve along the minimum energy path in the bending coordinate γ. And that is exactly what is seen in Fig. 9, where we depict the wave functions for various bending states up to $v_2=50$ corresponding to about 20 000 cm^{-1} above the ground state. Up to about $v_2=34$ the wave functions do not show distortions and are easy to locate in the spectrum. At higher energies, the bending states become more difficult to assign and the wave functions show gradually more admixtures of other states, which also shows up in noticeable deviations of $[E_{(0,v_2+2,0)}-E_{(0,v_2,0)}]$ from a smooth line. The reason is the increased density of states and the resulting coupling between all three modes.

This is in qualitative accord with the classical continuation–bifurcation diagram. The bending family of POs, $[B]$, is stable up to about 2 eV, which corresponds to ~32 quanta of the bending mode. It is checked that the POs scar the $(0,v_2,0)$ wave functions (first panel in Fig. 9). At a first bifurcation the $[B]$-type orbits become unstable and a new stable family comes into existence. However, the new stable POs quickly become unstable, too, and a cascade of additional bifurcations sets in. With other words, the structure of the classical phase space becomes quite complex, which makes it appear reasonable, why the higher overtones of the pure bending progression ($v_2>40$ or so) are perturbed.

Incidentally we note that the rotational constant B_{rot}, calculated as the expectation value of the inverse of the moment of inertia using the $J=0$ wave functions, steadily increases up to $v_2\approx 44$, as it is expected for linear molecules like HCP and DCP. In contrast, the same quantity for HCP *decreases* with v_2, except for the lowest bending excitations. This decrease for HCP results from the obstruction of the pure bending motion and the increasingly growing admixture of CP stretch motion.

VII. SUMMARY

(1) The vibrational energy level spectrum of DCP has been determined by quantum-mechanical variational calculations using an accurate potential energy surface. In order to assign the spectrum, all wave functions of the first five hundred states and selected wave functions at even higher energies have been visually inspected. The agreement of the calculated transition energies and rotational constants with the few available experimental data is excellent.

(2) Unlike the HCP spectrum, which is governed by a 2 : 1 HC stretch : bend anharmonic resonance, the spectrum of DCP is determined by a 2 : 1 HC stretch : CP stretch resonance. The resonance condition is best fulfilled at the lowest energies; however, because of the anharmonicity of the DC stretch mode, the mismatch between the two stretching (transition) frequencies increases with increasing energy. The bending degree of freedom is to a large extent decoupled from the other two modes. As a consequence of the resonance and the weak coupling between the bend and the two stretches, the energies are organized in terms of polyads for a particular bending quantum number. The assignment in terms of three quantum numbers is straightforward up to about 1.75 eV above the minimum energy. Then, a new class of wave functions gradually comes into existence, which does not fit into the scheme developed at lower energies.

(3) Analysis of the classical phase space—using the full Hamiltonian—in terms of periodic orbits and their continuation with increasing energy explains some of the features seen in the quantum-mechanical spectrum. For example, it is rationalized, that the wave functions of the two main stretching progressions, $(v_1,0,0)$ and $(0,0,v_3)$, follow two distinct types of stable periodic orbits, $[R]$ and $[R1]$, respectively. The latter are created in a very early bifurcation of the $[R]$ family, ~0.6 eV above minimum. The ''new'' states, termed $(0,0,v_3)_{\mathrm{r}}$, are shown to follow periodic orbits, which essentially correspond to CP stretching motion.

(4) Even more subtle details of the quantum mechanical spectrum are explained by a semiclassical analysis of a resonance Hamiltonian model, in which the parameters are obtained by fitting the exact quantum-mechanical energies.
(5) Because the bending mode is not involved in a resonance with the stretching degrees of freedom, the corresponding wave functions, analyzed up to state (0,50,0), do follow the DCP/CPD isomerization path. This is in striking disagreement with HCP, for which the states of the progression $(0,v_2,0)$ avoid the isomerization path. Thus, DCP is probably a more suitable candidate for studying how isomerization shows up in a spectrum.

ACKNOWLEDGMENTS

Financial support by the Deutsche Forschungsgemeinschaft through the Sonderforschungsbereich 357 ''Molekulare Mechanismen Unimolekularer Reaktionen'' and the Fonds der Chemischen Industrie is gratefully acknowledged. S.C.F. and R.S. are grateful to the Alexander von Humboldt–Stiftung for a travel grant. R.S. thanks S. Yu. Grebenshchikov for stimulating discussions and valuable comments on the manuscript.

[1] *Molecular Dynamics and Spectroscopy by Stimulated Emission Pumping*, edited by H.-L. Dai and R. W. Field (World Scientific, Singapore, 1995).
[2] M. J. Davis, Int. Rev. Phys. Chem. **14**, 15 (1995).
[3] M. E. Kellman, Int. J. Quantum Chem. **65**, 399 (1997).
[4] D. Papousek and M. R. Aliev, *Molecular Vibrational-Rotational Spectra* (Elsevier, Amsterdam, 1982).
[5] C. C. Martens and G. S. Ezra, J. Chem. Phys. **86**, 279 (1987).
[6] M. E. Kellman, in *Molecular Dynamics and Spectroscopy by Stimulated Emission Pumping*, edited by H.-L. Dai and R. W. Field (World Scientific, Singapore, 1995).
[7] M. Joyeux, Chem. Phys. **203**, 281 (1996).
[8] J. Guckenheimer and P. Holmes, *Nonlinear Oscillations, Dynamical Systems, and Bifurcations of Vector Fields* (Springer-Verlag, Berlin, 1983).
[9] H. Ishikawa, Y.-T. Chen, Y. Ohshima, J. Wang, and R. W. Field, J. Chem. Phys. **105**, 7383 (1996).
[10] S. C. Farantos, H.-M. Keller, R. Schinke, K. Yamashita, and K. Morokuma, J. Chem. Phys. **104**, 10055 (1996).
[11] C. Beck, H.-M. Keller, S. Yu. Grebenshchikov, R. Schinke, S. C. Farantos, K. Yamashita, and K. Morokuma, J. Chem. Phys. **107**, 9818 (1997).
[12] H. Ishikawa, R. W. Field, S. C. Farantos, M. Joyeux, J. Koput, C. Beck, and R. Schinke, Annu. Rev. Phys. Chem. **50**, 443 (1999).
[13] H. Ishikawa, C. Nagao, N. Mikami, and R. W. Field, J. Chem Phys. **106**, 2980 (1997).
[14] C. Beck, R. Schinke, and J. Koput (in preparation).
[15] S. C. Farantos, C. Beck, and R. Schinke, Theor. Chem. Acc. **100**, 147 (1998).
[16] A. J. Dobbyn, M. Stumpf, H.-M. Keller, and R. Schinke, J. Chem. Phys. **103**, 9947 (1995).
[17] C. Puzzarini, R. Tarroni, P. Palmieri, J. Demaison, and M. L. Senent, J. Chem. Phys. **105**, 3132 (1996).
[18] J. Lavigne, C. Pépin, and A. Cabana, J. Mol. Spectrosc. **99**, 203 (1983).
[19] J. Lavigne, C. Pépin, and A. Cabana, J. Mol. Spectrosc. **104**, 49 (1984).
[20] C. Pépin and A. Cabana, J. Mol. Spectrosc. **119**, 101 (1986).
[21] See EPAPS Document No. E-JCPSA6-112-001020 for a complete list of the first thousand energy levels and assignments. This document contains also postscript files of the figures of wave functions for $v_2=2$ and 4 (corresponding to Figs. 2 and 3 for $v_2=0$). This document may be retrieved via the EPAPS homepage (http://www.aip.org/pubservs/epaps.html) or from ftp.aip.org in the directory /epaps/. See the EPAPS homepage for more information.
[22] P. Botschwina and P. Sebald, J. Mol. Spectrosc. **100**, 1 (1983).
[23] M. E. Kellman, Annu. Rev. Phys. Chem. **46**, 395 (1995).
[24] J. Weiß, J. Hauschildt, S. Yu. Grebenshchikov, R. Düren, R. Schinke, J. Koput, S. Stamatiadis and S. C. Farantos, J. Chem. Phys. **112**, 77 (2000).
[25] S. C. Farantos, Int. Rev. Phys. Chem. **15**, 345 (1996).
[26] H. S. Taylor, in *Molecular Dynamics and Spectroscopy by Stimulated Emission Pumping*, edited by H.-L. Dai and R. W. Field (World Scientific, Singapore, 1995).
[27] E. J. Heller and S. Tomsovic, Phys. Today **46**, 38 (1993).
[28] G. Contopoulos, Astron. J. **75**, 96 (1970).
[29] S. C. Farantos, Comput. Phys. Commun. **108**, 240 (1998).
[30] M. Joyeux, S. Yu. Grebenshchikov, and R. Schinke, J. Chem. Phys. **109**, 8342 (1998).
[31] M. Joyeux, D. Sugny, V. Tyng, M. E. Kellman, H. Ishikawa, R. W. Field, C. Beck, and R. Schinke, J. Chem. Phys. **112**, 4162 (2000).
[32] R. Jost, M. Joyeux, S. Skokov, and J. M. Bowman, J. Chem. Phys. **111**, 6807 (1999).
[33] M. Joyeux, J. Chem. Phys. **109**, 2111 (1998).
[34] V. P. Maslov and M. V. Fedoriuk, *Semiclassical Approximations in Quantum Mechanics* (Deidel, Dordrecht, 1981).
[35] M. Golubistsky and D. G. Schaeffer, *Singularities and Groups in Bifurcation Theory*, Vol. I (Springer, New York, 1981).
[36] Z. Li, L. Xiao, and M. E. Kellman, J. Chem. Phys. **92**, 2251 (1990).